J. Fluid Mech. (1980), *vol.* 101, *part* 2, *pp.* 349–376
Printed in Great Britain

Dynamical cascade models for Kolmogorov's inertial flow

By JON LEE
Flight Dynamics Laboratory, Wright–Patterson AFB, Ohio 45433

(Received 5 March 1979)

To resolve possible fluctuations about the mean motion of the Desnyansky–Novikov model for Kolmogorov's inertial flow, we have investigated two dynamical systems of the cascade process which are formally derivable from Burgers' equation. The first cascade model produced no fluctuations, for its trajectory was identical with the Desnyansky–Novikov model's. Disappointingly, the second cascade system, which is similar to the Kerr–Siggia model, has also proved unable to engender fluctuations. This is because the second model when truncated consistently maps an arbitrary initial point into the attainable phase space of the first cascade model. However, when truncated inconsistently the trajectory of second model can exhibit a quite erratic and somewhat sporadic motion, thereby reflecting the apparently random motion of inviscid equilibrium solutions. Therefore, the observation of temporally intermittent fluctuations by a stationary Kerr–Siggia model is due to the inconsistent truncation produced by restricting energy dissipation for all but the upper truncation mode in their model.

1. Statement of the problem

To provide some theoretical justification for Kolmogorov's inertial flow, Desnyansky & Novikov (1974*a*, *b*) proposed a dynamical model for the underlying cascade process that can correctly reproduce the $-\frac{5}{3}$ spectral law. Since the velocity field will be assumed spherically symmetric in statistical sense, it suffices to consider here the energy spectrum $E(k)$ of isotropic turbulence. Suppose that we inscribe in the three-dimensional wave-vector space a sequence of spherical shells, the radii of which increase successively by twofold. To be specific, for a given wavenumber k we introduce the spherical shells of radii, ..., $k/2\sqrt{2}$, $k/\sqrt{2}$, $\sqrt{2}\,k$, $2\sqrt{2}\,k$, ... We then define the average modal energy $\frac{1}{2}v^2(k)$ over the adjacent shells of radii $k/\sqrt{2}$ and $\sqrt{2}\,k$ by

$$\tfrac{1}{2}v^2(k) = \int_{k/\sqrt{2}}^{\sqrt{2}\,k} E(k')\,dk'. \tag{1.1}$$

The average energies $\frac{1}{2}v^2(\frac{1}{2}k)$ and $\frac{1}{2}v^2(2k)$ are defined similarly over the adjacent shells of radii $k/2\sqrt{2}$ and $k/\sqrt{2}$, and of radii $\sqrt{2}\,k$ and $2\sqrt{2}\,k$, respectively. The Desnyansky–Novikov model takes into account only the interaction of $v(k)$ with $v(k/2)$ and $v(2k)$ as follows;

$$(\partial/\partial t + \nu\beta(k)\,k^2)\,v(k) = \gamma k[v^2(k/2) - 2v(k)\,v(2k)] + F(k). \tag{1.2}$$

Here ν is the kinematic viscosity, γ measures the strength of quadratic interactions, the yet unspecified $\beta(k)$ corrects for shell-averaged damping, and $F(k)$ is the energy

0022-1120/80/4548-2370 $02.00

input term (see Bell & Nelkin 1977, 1978 for extensions of model (1.2)). Suppose that $F(k)$ acts on the very small k, whereas energy dissipation takes place predominantly in the very high wavenumber range, for ν is assumed small. Then, in the intermediate k range it is found that (1.2) can equilibrate toward a steady state $v \sim k^{-\frac{1}{3}}$, which satisfies $v^2(\frac{1}{2}k) - 2v(k)\,v(2k) = 0$. Hence, the equilibrium energy distribution is of the form

$$v^2(k) \sim k^{-\frac{2}{3}}. \tag{1.3}$$

Since this implies $E(k) \sim k^{-\frac{5}{3}}$ by definition (1.1), it was claimed that (1.2) is a dynamical cascade model for Kolmogorov's inertial flow. Although it is gratifying to recover the $-\frac{5}{3}$ spectral law by a simple model such as (1.2), the achievement of the Desnyansky–Novikov model is in our opinion a fortuitous accident. This is because, in spite of some recent attempts by Siggia (1977, 1978), the cascade model (1.2) is not derivable from the Navier–Stokes equations; hence the nonlinear terms have been constructed heuristically by requiring (i) quadratic nonlinearity, (ii) scale invariance to dimensionless coefficients, (iii) direct coupling of the closest neighbouring modes and (iv) energy conservation.

Instead of invoking the aforementioned requirements, one can formally derive the cascade model (2.9) which has an equilibrium energy distribution of the form (1.3) (see § 2). Although (2.9) has the same form as the Desnyansky–Novikov model, they are by no means identical; they describe in fact two different processes. On the one hand, (1.2) refers to modal energies averaged over the two adjacent shells; hence Kolmogorov's spectral law follows at once by invoking definition (1.1). On the other hand, (2.9) refers to the actual cascade process itself. Consequently, an ensemble of realizations (2.9) would represent the mean motion of the Desnyansky–Novikov model. Viewed as description of a realization, one cannot therefore deduce from (2.10) the $-\frac{5}{3}$ spectral law because (1.1) is no longer operative. A way around this difficulty was suggested (J. Lee 1971, unpublished note: Kolmogorov's similarity law of the inertial subrange spectrum) by heuristically introducing a factor α^{-1} into (2.10), which is the usual procedure for converting a plane wave to the three-dimensional spherical wave. This issue aside, the real motive for investigating (2.9) as a cascade process is to uncover possible fluctuations which might have been averaged out in the Desnyansky–Novikov model. Although such a hope is not realized by (2.9), the dynamical cascade equations when generalized to the complex mode appear to have sufficiently complicated trajectory behaviour to create random fluctuations about the Desnyansky–Novikov model.

With this in mind, Kerr & Siggia (1978) have recently proposed the complex extension of (2.9). Clearly, the cascade model (3.1) with complex modes is richer in dynamical properties than the real-mode counterpart (2.9). In the inviscid limit, (3.1) is measure-preserving. Further, it has only two isolating constants of motion: energy and a cubic constant of motion h (see § 3.1). For a given energy, h can take any value from zero to a maximum. It has been shown that the maximum and zero h give rise to the invariant sets $\mathscr{S}_m$ and $\mathscr{S}_0$, respectively (§ 3.2). First, $\mathscr{S}_m$ is a trivial equilibrium point which can never be attained from any other points in the phase space. The second invariant set $\mathscr{S}_0$ is relevant to the discussion of this paper; it represents the attainable phase space of dynamical system (2.9).

As a preliminary, we have investigated truncated systems of inviscid model (3.1),

which is identical to the inviscid Kerr–Siggia model, on a constant energy and h surface (§ 4). It is very surprising to note that, as the dimension of truncation is increased from 3 to 4, the motion of the inviscid Kerr–Siggia model suddenly changes from periodic or quasi-periodic to non-periodic. Then the non-periodic trajectory becomes more and more random as the order of truncation is increased. In fact, the random trajectory of higher-order modes almost develops mixing in phase space, whereas the lower-order modes undergo a gradual but somewhat sporadic non-periodic motion. Therefore, a layered structure of the inviscid Kerr–Siggia model emerges. Slowly evolving big eddies (lower-order modes) coexist with small eddies (higher-order modes); the trajectory of these eddies becomes progressively more chaotic with the decreasing eddy size. What is apparent here is the decrease in characteristic time with the decreasing eddy size. In the inviscid case, all modes participate energetically as evidenced by energy sharing of the time-averaged modal energies.

The knowledge of inviscid equilibrium solutions is not at all unproductive. On the contrary, it permits us to resolve the problem of inconsistent truncation, when the cascade model (3.1) is held stationary by injecting energy at the same rate as the energy dissipation. Although (3.1) is an unclosed system, based on a Kolmogorov dissipation length scale one may choose an upper truncation wavenumber so large that the contribution of all truncated modes is negligible. Such a truncation is said to be consistent. The consistently truncated model (3.1) has a very surprising long-time behaviour. It evolves an arbitrary initial point into the invariant set $\mathscr{S}_0$ (§ 5.2). In other words, the equilibrium state of (3.1) is identical to the steady equilibrium point of (2.9), which is (1.3). Now, if the truncation wavenumber is smaller than a Kolmogorov dissipation wavenumber, the viscous effects are grossly inhibited so that the equilibrium state will be dominated by inviscid solutions (Orszag 1977). Indeed, the trajectory of an inconsistently truncated (3.1) exhibits the apparently random motion of inviscid solutions superimposed on the otherwise stable (non-random) motion of the invariant set $\mathscr{S}_0$ (§ 5.2). Kerr & Siggia (1978) have observed that their model can develop temporally intermittent fluctuations about the mean motion of the Desnyansky–Novikov model. We believe that such an observation is the direct consequence of inconsistent truncation, whereby only the upper truncation mode is allowed to dissipate energy by an artificial eddy damping.

2. The cascade model with real modes

We begin with Burgers' equation

$$\partial u/\partial t + \tfrac{1}{2}\,\partial u^2/\partial x - \nu\,\partial^2 u/\partial x^2 = 0 \tag{2.1}$$

in the spatial interval of $[0, L]$. For a flow field satisfying the boundary condition $u(0) = u(L) = 0$, one can introduce

$$u(x,t) = \sum_{\alpha=1}^{\infty} \xi_\alpha(t) \sin(\alpha\pi x/L),$$

into (2.1), thereby extracting the infinite set of Fourier amplitude equations

$$(\partial/\partial t + \nu(\alpha\pi/L)^2)\,\xi_\alpha = (\alpha\pi/2L)\left[\sum_{\beta=1}^{\infty} \xi_\beta \xi_{\alpha+\beta} - \frac{1}{2}\sum_{\beta=1}^{\alpha-1} \xi_\beta \xi_{\alpha-\beta}\right]. \tag{2.2}$$

It will be shown that the quadratic terms can be separated into two dynamical processes, the unidirectional energy transfer and triad energy exchange (§ 2.1). The cascade model is then a typical representation of the unidirectional energy flow process (§ 2.2).

2.1. *Classification of nonlinear processes*

We shall now suppress the viscous term. The structure of the quadratic terms can be exhibited most clearly by rearranging the right-hand side of (2.2) under $L = \pi$ as follows,

$$\begin{pmatrix} \dot{\xi}_1 \\ \dot{\xi}_2 \\ \dot{\xi}_3 \\ \dot{\xi}_4 \\ \dot{\xi}_5 \\ \vdots \end{pmatrix} = \frac{1}{2}\left\{ \begin{pmatrix} \xi_1\xi_2 \\ -\xi_1^2 \\ 0 \\ 0 \\ 0 \\ \vdots \end{pmatrix} + \begin{pmatrix} \xi_2\xi_3 \\ 2\xi_1\xi_3 \\ -3\xi_1\xi_2 \\ 0 \\ 0 \\ \vdots \end{pmatrix} + \begin{pmatrix} \xi_3\xi_4 \\ 2\xi_2\xi_4 \\ 3\xi_1\xi_4 \\ -4\xi_1\xi_3 - 2\xi_2^2 \\ 0 \\ \vdots \end{pmatrix} + \ldots \right\}$$

$$\equiv \tfrac{1}{2}\{\boldsymbol{\Phi}_1 + \boldsymbol{\Phi}_2 + \boldsymbol{\Phi}_3 + \ldots\}, \tag{2.3}$$

where the dot denotes $\partial/\partial t$. Since each of the column vectors $\boldsymbol{\Phi}_\alpha$ is orthogonal to the vector $(\xi_1, \xi_2, \xi_3, \ldots)$, a truncation that excludes any (but not all) of $\boldsymbol{\Phi}_\alpha$ will conserve its energy.

The unidirectional energy transfer. The lowest-order truncation excludes all but $\boldsymbol{\Phi}_1$:

$$\dot{\xi}_1 = \tfrac{1}{2}\xi_1\xi_2, \quad \dot{\xi}_2 = -\tfrac{1}{2}\xi_1^2. \tag{2.4}$$

By the transformation $\xi_1 = \exp(\frac{1}{2}y)$ and $\xi_2 = z$ (I am indebted to Henry Fettis for this), (2.4) gives rise to an equation of the Emden type, $\ddot{y} + \frac{1}{2}\exp(y) = 0$ (Kamke 1943, p. 562). Hence the solution satisfying the energy conservation $\xi_1^2 + \xi_2^2 = 1$ is

$$\xi_1 = \operatorname{sech}[\tfrac{1}{2}(t - t_0)], \quad \xi_2 = -\tanh[\tfrac{1}{2}(t - t_0)]. \tag{2.5}$$

Here the constant t_0 is chosen to satisfy the initial condition. Since $\xi_1^2 = 0$ and $\xi_2^2 = 1$ as $t \to \infty$, (2.4) describes the eventually complete transfer of the first-mode energy to ξ_2. Hence, the term 'unidirectional energy transfer' is justified.

The triad energy exchange. The three-mode interaction is exhibited by including only $\boldsymbol{\Phi}_2$ in (2.3),

$$\dot{\xi}_1 = \tfrac{1}{2}\xi_2\xi_3, \quad \dot{\xi}_2 = \xi_1\xi_3, \quad \dot{\xi}_3 = -\tfrac{3}{2}\xi_1\xi_2. \tag{2.6}$$

The solution can be expressed by the Jacobian elliptic functions

$$\xi_1 = a_1 \operatorname{cn}[\lambda(t - t_0), \kappa], \quad \xi_2 = a_2 \operatorname{dn}[\lambda(t - t_0), \kappa], \quad \xi_3 = -a_3 \operatorname{sn}[\lambda(t - t_0), \kappa], \tag{2.7}$$

where t_0 is the initial time. The constants are related by $2a_1^2 = \kappa^2 a_2^2 = \frac{2}{3}a_3^2 = a_1 a_2 a_3/\lambda$, and $a_1^2 + a_2^2 = 1$ due to the energy conservation. If the modulus κ turns out to be greater than 1, then by the reciprocal modulus transformation (Byrd & Friedman 1954, p. 38) we can write the alternative form $\xi_1 \sim \mathrm{dn}$, $\xi_2 \sim \mathrm{cn}$, and $\xi_3 \sim \mathrm{sn}$ with the corresponding modulus less than 1. Since the Jacobian elliptic functions are periodic, (2.6) represents the three-mode (triad) energy exchange under $\xi_1^2 + \xi_2^2 + \xi_3^2 = 1$. Although Lorenz (1960) appears to be the first to have discussed the triad system (2.6) in connexion with fluid dynamics, it is essentially Euler's equations for a rigid body moving with one point fixed under no external forces. (Lamb (1943, p. 123) has given credit to St. A. Reub (1834) for the analytic solution (2.7).)

Summing up, $\mathbf{\Phi}_1$ represents the unidirectional flow of energy from ξ_1 to ξ_2, which will be denoted by $\xi_1 \Rightarrow \xi_2$. On the other hand, $\mathbf{\Phi}_2$ describes the periodic energy exchange among ξ_1, ξ_2 and ξ_3. One can readily interpret the remaining vectors $\mathbf{\Phi}_\alpha$ in terms of the two dynamic processes. For instance, $\mathbf{\Phi}_3$ represents $\xi_2 \Rightarrow \xi_4$ and a triad energy exchange among ξ_1, ξ_3, and ξ_4. And $\mathbf{\Phi}_4$ represents the triad energy exchange between ξ_1, ξ_4 and ξ_5 coupled to another one between ξ_2, ξ_3 and ξ_5.

2.2. *The cascade model*

It is strongly suspected that by sequentially coupling $\xi_1 \Rightarrow \xi_2$ and $\xi_2 \Rightarrow \xi_4$ the first-mode energy might all be transferred to ξ_4. The dynamical equations for such a sequential energy flow $\xi_1 \Rightarrow \xi_2 \Rightarrow \xi_4$ is

$$\dot{\xi}_1 = \tfrac{1}{2}\xi_1\xi_2, \quad \dot{\xi}_2 = -\tfrac{1}{2}\xi_1^2 + \xi_2\xi_4, \quad \dot{\xi}_4 = -\xi_2^2. \tag{2.8}$$

A numerical solution of (2.8) has indeed confirmed this suspicion. As shown in figure 1, the initial energy $\xi_1^2 = 1$ eventually becomes transferred to ξ_4 but with the ephemeral excitation of ξ_2. Expanding (2.8) to include $\xi_4 \Rightarrow \xi_8$ and $\xi_8 \Rightarrow \xi_{16}$ and so on, we obtain the dynamical equations of the cascade process as follows:

$$\left.\begin{aligned} \dot{\xi}_1 + \nu\xi_1 &= \epsilon_f/\xi_1 + \tfrac{1}{2}\xi_1\xi_2, \\ \dot{\xi}_2 + \nu 2^2\xi_2 &= \tfrac{1}{2}(-\xi_1^2 + 2\xi_2\xi_3), \\ \dot{\xi}_3 + \nu 4^2\xi_3 &= -\xi_2^2 + 2\xi_3\xi_4, \\ &\vdots \\ \dot{\xi}_n + \nu(2^{n-1})^2\xi_n &= 2^{n-3}(-\xi_{n-1}^2 + 2\xi_n\xi_{n+1}) \quad (n \geqslant 2). \end{aligned}\right\} \tag{2.9}$$

The following comments are in order. (i) We have redefined ξ_α ($\alpha = 1, 2, 4, 8, \ldots$) by ξ_n ($n = 1, 2, 3, \ldots$), the relabelling relation being $\alpha = 2^{n-1}$. (ii) Since we let $L = \pi$, α is the wavenumber. (iii) The viscous term has been reintroduced. Otherwise, the equilibrium solution of (2.9) is simply the piling up of all modal energies on the upper truncation mode. (iv) Finally, in the first of (2.9) the term ϵ_f/ξ_1 is the analytical statement that energy is being fed into the first mode at the rate ϵ_f (Kerr & Siggia 1978).

Let us define a dissipation wavenumber in terms of Kolmogorov's length scale by $\alpha_k = (\epsilon_\nu/\nu^3)^{\frac{1}{4}}$, where ϵ_ν is the energy dissipation rate. Introduce an upper truncation limit n_t with the corresponding wavenumber $\alpha_t = 2^{n_t-1}$. If n_t is so large that $\alpha_t \gg \alpha_k$, the truncated modes will all lie in the wavenumber range of strong dissipation so that their contribution can safely be ignored. Such a truncation will be said to be consistent. In the opposite case of $\alpha_t \ll \alpha_k$, however, the viscous effects are grossly inhibited (Orszag 1977). Hence, an inconsistent truncation will falsely identify the inviscid solution (i.e. the piling up of all modal energies on the ξ_{n_t}) with the stationary equilibrium state of (2.9). Suppose now that (2.9) is truncated consistently. Since energy is continually introduced into ξ_1 (the largest eddy) and since energy is dissipated mostly by the higher-order ξ_n (smaller eddies), (2.9) can simulate the cascade flow of energy down the eddies, which decrease in size successively by half. It is known that (Lee 1971, unpublished note; Desynansky & Novikov 1974*a*) equilibration is possible for the eddies not directly affected by the energy input and viscous damping. Since (2.9) reduces to $\dot{\xi}_n = 2^{n-3}(-\xi_{n-1}^2 + 2\xi_n\xi_{n+1})$ for $2 < n < n_t$, the steady-state solution is

$$\xi_n = c_1 2^{-\frac{1}{3}n},$$

or, in the original variables, we have

$$\xi_\alpha = c_2\alpha^{-\frac{1}{3}},$$

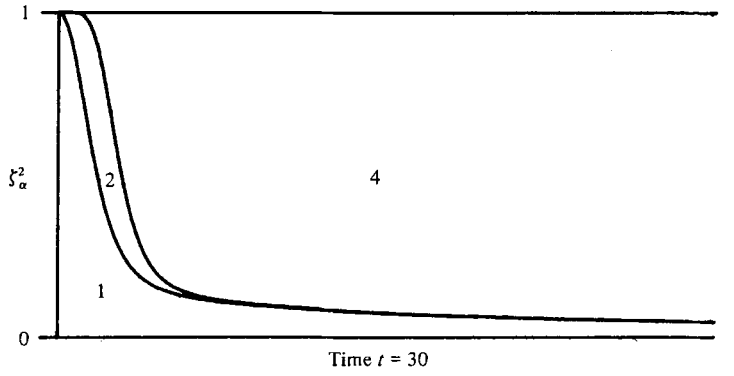

FIGURE 1. Modal energies of (2.8) evolved from the initial condition $\xi_1 = 1$ and $\xi_2 = \xi_4 = 0$; note that 1, 2, and 4 refer to the subscript α. (The unidirectional energy transfer is very slow; only 99 % of total energy is transferred to ξ_4 at $t = 200$.)

where c_1 and c_2 are constants. Hence, the equilibrium modal energy distribution obeys

$$\xi_\alpha^2 \sim \alpha^{-\frac{2}{3}}. \tag{2.10}$$

Although ν does not appear explicitly, (2.10) is indeed a viscous solution. Note that ν dictates the wavenumber range in which (2.10) is valid, which extends farther as ν becomes small but not zero. In the inviscid case ($\nu = 0$), however, (2.10) is no longer valid; the corresponding equilibrium state is the inviscid solution. (The dynamical difference between the limit as $\nu \to 0$ and the inviscid case has been discussed by Orszag (1977).)

The stability and attainability of (2.10) have been checked out by directly integrating (2.9) under $n_t = 11$ and $\nu = 1 \times 10^{-4}$. Since ϵ_f necessary for equilibration is not known *a priori*, a practical procedure is to boost ξ_1 at the end of each integration time step to maintain

$$\sum_{n=1}^{11} \xi_n^2 = 1.$$

The ratio of energy injected to the time step is then ϵ_f. Figure 2(*a*) demonstrates two things: In the first time range ($0 \leqslant t < 15$), the initial condition

$$I_1 = \{\xi_1 = 1, \xi_n = 0\,(2 \leqslant n \leqslant 11)\}$$

develops rapidly into the equilibrium energy state. In the second time range ($15 \leqslant t \leqslant 30$), however, this equilibrium state is shown to re-establish after having perturbed the three modes at $t = 15$ as follows. The ξ_3 and ξ_5 are reduced by 30 % and 50 %, respectively, but ξ_4 is increased to maintain

$$\sum_{n=1}^{11} \xi_n^2 = 1.$$

As expected, in equilibrium ϵ_f is equal to the energy dissipation rate computed by

$$\epsilon_\nu = 2\nu \sum_{n=1}^{11} 2^{2(n-1)} \xi_n^2.$$

Using $\epsilon_f = \epsilon_\nu \simeq 0{\cdot}183$, we find that the Kolmogorov $\alpha_k \simeq 65{\cdot}4$ is well below the

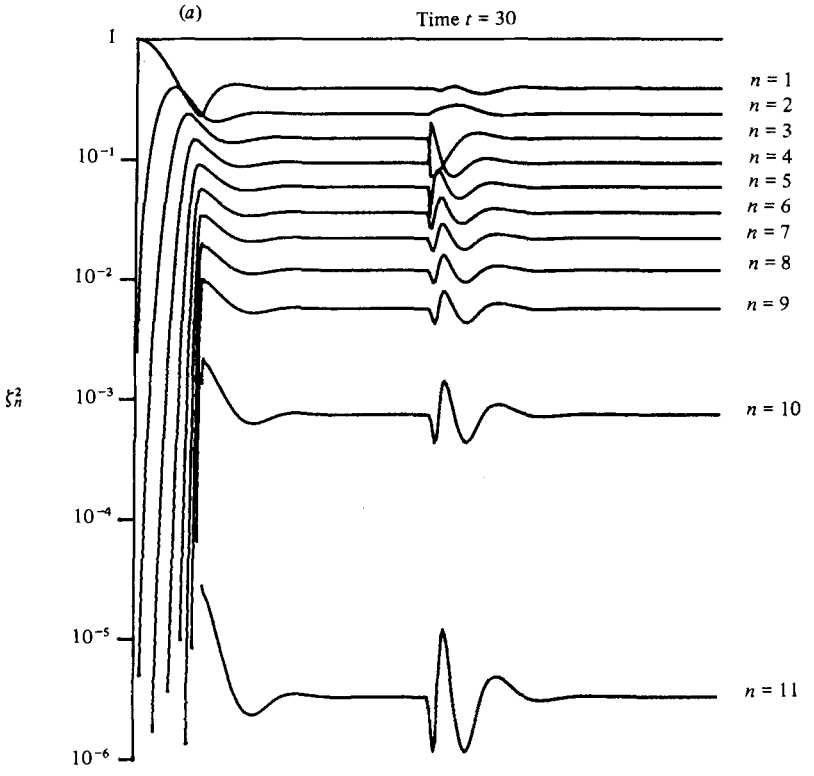

Caption for figure 2(*a*) over page.

truncation $\alpha_t = 1024$; hence the present truncation is certainly consistent. The equilibrium energy distribution shown in figure 2(*b*) obeys the $-\frac{2}{3}$ power form up to $n = 7$ ($\alpha = 64$), beyond which the viscous dissipation is significant. Numerical experimentation has shown that (2.10) is attainable from an arbitrary initial condition with $\xi_1 \neq 0$.

We wish to point out that (2.9) is but one of infinitely many cascade models embedded in Burgers' equation. For instance, the second model is

$$\xi_3 \Rightarrow \xi_6 \Rightarrow \xi_{12} \Rightarrow \xi_{24} \Rightarrow \ldots,$$

and the remaining cascade models are constructed by commencing from the modes ξ_7, ξ_{11}, etc.

3. The cascade model with complex modes

Recently, Kerr & Siggia (1978) have proposed the complex extension of (2.9), which is obtained by introducing into Burgers' equation the Fourier expansion appropriate for cyclic boundary conditions

$$u(x,t) = \sum_{\alpha=-\infty}^{\infty} u_\alpha(t) \exp(2i\alpha\pi x/L).$$

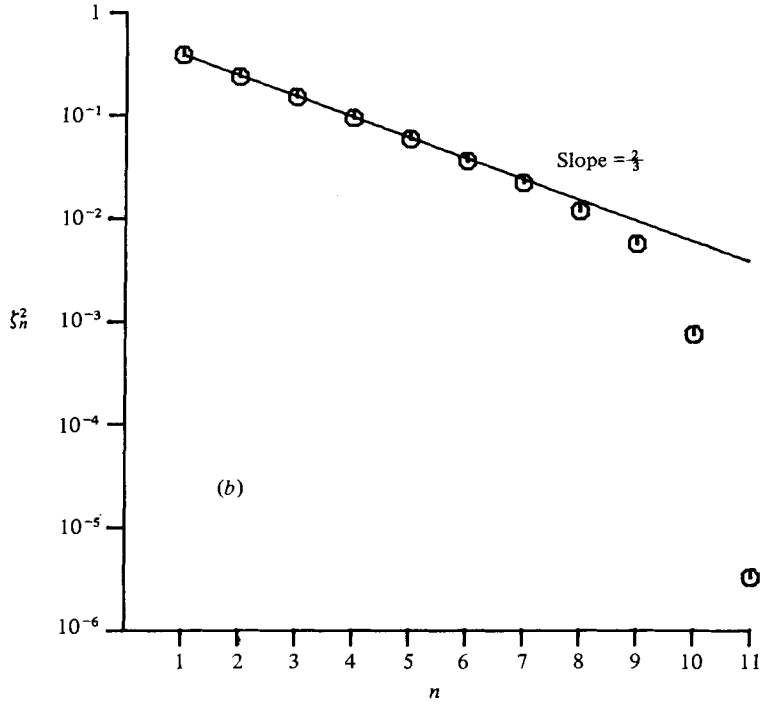

FIGURE 2. Evolution of (2.9) from the initial condition I_1 under $n_t = 11$ and $\nu = 1 \times 10^{-4}$. (*a*) Development and re-establishment of the equilibrium energy state. At $t = 15$, ξ_3 and ξ_5 are decreased by 30 % and 50 %, respectively, and ξ_4 is increased to maintain $\Sigma_{n=1}^{11} \xi_n^2 = 1$. (*b*) Equilibrium modal energies at the final time ($t = 30$).

The reality requirement demands that $u_\alpha^*(t) = u_{-\alpha}(t)$. Patterning after (2.9) the cascade model with complex modes becomes

$$\left.\begin{aligned} \dot{u}_1 + \nu u_1 &= \epsilon_f/u_1^* - iu_1^* u_2, \\ \dot{u}_2 + \nu 2^2 u_2 &= -i(u_1^2 + 2u_2^* u_3), \\ \dot{u}_3 + \nu 4^2 u_3 &= -i2(u_2^2 + 2u_3^* u_4), \\ &\vdots \\ \dot{u}_n + \nu(2^{n-1})^2 u_n &= -i2^{n-2}(u_{n-1}^2 + 2u_n^* u_{n+1}) \quad (n \geqslant 2). \end{aligned}\right\} \tag{3.1}$$

Although (3.1) shares the same nonlinear terms with the Kerr–Siggia model (equations (13) in Kerr & Siggia 1978), there are two differences. The first is a minor one: the constant factor for the nonlinear terms in (3.1) differs from that of the Kerr–Siggia model by -2. The second difference, however, has a very important implication. The viscous terms $\nu(2^{n-1})^2 u_n$ are the natural ones arising from $\nu \partial^2 u/\partial x^2$ in (2.1). In contrast, the Kerr–Siggia model relegates all viscous dissipation only to the upper truncation mode via an artificial eddy-damping term. This will therefore restrict the natural flow of energy towards the Kolmogorov dissipation range. These differences, however, disappear in the inviscid flow case to be discussed in this section.

3.1. *Inviscid invariants of motion*

Prior to investigation of (3.1), it behooves us to examine the inviscid dynamics under no external excitation ($\nu = \epsilon_f = 0$). Since it makes no sense to discuss (3.1) in its entirety in the inviscid case, we shall truncate it at n_t:

$$\left.\begin{aligned} \dot{u}_1 &= -iu_1^* u_2, \\ \dot{u}_n &= -i2^{n-2}(u_{n-1}^2 + 2u_n^* u_{n+1}) \quad (2 \leqslant n < n_t), \\ \dot{u}_{n_t} &= -i2^{n_t-2} u_{n_t-1}^2. \end{aligned}\right\} \tag{3.2}$$

First, this system conserves energy which for convenience is normalized as

$$\sum_{n=1}^{n_t} |u_n|^2 = 1.$$

Second, as pointed out by Kerr & Siggia (1978), there is a cubic constant of motion

$$h = \sum_{n=1}^{n_t-1} \mathrm{Re}\,(u_n^2 u_{n+1}^*).$$

Finally, (3.2) preserves measure under the time evolution because

$$\sum_{n=1}^{n_t} \partial \dot{u}_n^r / \partial u_n^r + \partial \dot{u}_n^i / \partial u_n^i = 0,$$

where $u_n = u_n^r + iu_n^i$. Hence it obeys the classical Liouville theorem.

3.2. *Invariant sets*

Much can be learned by simply recasting (3.2) into the action-angle representation. Let us introduce $u_n = R_n \exp(i2\pi\omega_n)$ into (3.2), and separate out the real and imaginary parts

$$\left.\begin{aligned} \dot{R}_1 &= R_1 R_2 \sin(2\pi\Omega_1), \\ \dot{R}_2 &= -R_1^2 \sin(2\pi\Omega_1) + 2R_2 R_3 \sin(2\pi\Omega_2), \\ \dot{R}_3 &= -2R_2^2 \sin(2\pi\Omega_2) + 4R_3 R_4 \sin(2\pi\Omega_3), \\ \dot{R}_4 &= -4R_3^2 \sin(2\pi\Omega_3) + 8R_4 R_5 \sin(2\pi\Omega_4), \\ &\vdots \\ 2\pi\dot{\Omega}_1 &= (2R_2 - R_1^2/R_2)\cos(2\pi\Omega_1) - 2R_3 \cos(2\pi\Omega_2), \\ 2\pi\dot{\Omega}_2 &= 2R_1^2/R_2 \cos(2\pi\Omega_1) + 2(2R_3 - R_2^2/R_3)\cos(2\pi\Omega_2) - 4R_4 \cos(2\pi\Omega_3), \\ 2\pi\dot{\Omega}_3 &= 4R_2^2/R_3 \cos(2\pi\Omega_2) + 4(2R_4 - R_3^2/R_4)\cos(2\pi\Omega_3) - 8R_5 \cos(2\pi\Omega_4), \\ &\vdots \end{aligned}\right\} \tag{3.3}$$

where $\Omega_n = \omega_{n+1} - 2\omega_n$. Since each mode u_n is represented by the amplitude R_n and angle ω_n, (3.3) describes the nonlinear dynamics of n_t oscillators or rotating vectors in the phase space of $\mathrm{Re}\,(u_n)$ *vs.* $\mathrm{Im}\,(u_n)$. The energy conservation

$$\sum_{n=1}^{n_t} J_n = 1$$

is expressed by the action $J_n\,(= R_n^2)$, and the cubic constant of motion becomes

$$h = \sum_{n=1}^{n_t-1} R_n^2 R_{n+1} \cos(2\pi\Omega_n).$$

Now, the two invariant sets of (3.3) can be deduced as follows. For the first, suppose that initially we choose ω_n such that $\Omega_n = \pm\frac{1}{4}, \pm\frac{3}{4}, \ldots$. It is then evident that ω_n will remain invariant because not only $\dot{\Omega}_n = 0$ but also $\dot{\omega}_n = 0$ for all t. Since

$$\sin(2\pi\Omega_n) = 1,$$

the R_n equations of (3.3) degenerate to the cascade model (2.9) (with $\epsilon_f = \nu = 0$). We shall denote this invariant set by $\mathscr{S}_0$, the zero subscript signifying $h = 0$ for such ω_n:

$$\mathscr{S}_0 = \{R_n \text{ satisfying the cascade model (2.9), and } \omega_n \text{ such that } \Omega_n = \pm\tfrac{1}{4}, \pm\tfrac{3}{4}, \pm\tfrac{5}{4}, \ldots\}. \tag{3.4}$$

Although (3.4) has been defined in the context of $\nu = \epsilon_f = 0$, it turns out that an invariant set defined exactly as $\mathscr{S}_0$ but with $\nu \neq 0$ and $\epsilon_f \neq 0$ plays an important role in § 5. We shall therefore represent by (3.4) both of these cases; however, no confusion arises as to which of the two cases is referred. The second invariant set is a trivial equilibrium state. Initially, we choose ω_n such that $\Omega_n = 0, \pm\frac{1}{2}, \pm 1, \ldots$ and also choose R_n such that the right-hand sides of Ω_n equations are identically zero; i.e.

$$\left.\begin{aligned} 2R_2 - R_1^2/R_2 - 2R_3 &= 0, \\ R_1^2/R_2 + 2R_3 - R_2^2/R_3 - 2R_4 &= 0, \\ R_2^2/R_3 + 2R_4 - R_3^2/R_4 - 2R_5 &= 0, \quad \ldots . \end{aligned}\right\} \tag{3.5}$$

It is evident that such a state will persist, for $\dot{R}_n = \dot{\Omega}_n = 0$ for all t. Since h then takes the maximum value, this invariant set will be denoted by the subscript m,

$$\mathscr{S}_m = \{R_n \text{ constrained by (3.5), and } \omega_n \text{ such that } \Omega_n = 0, \pm\tfrac{1}{2}, \pm 1, \ldots\}. \tag{3.6}$$

The existence of $\mathscr{S}_0$ and $\mathscr{S}_m$ establishes the two isolated equilibrium states, corresponding respectively to the zero and maximum h. Between the two limiting values of h, however, the trajectory of (3.3) can develop a random motion, as we shall explore in the next section.

4. The random motion of truncated inviscid systems

The polar representation (3.3) is not amenable to numerical integration because of the reciprocal factors R_n^{-1} which appear ubiquitously in the Ω_n equations (Lee 1979). Hence, we shall integrate the system (3.2), even though dynamical results are discussed alternately in action-angle variables. We denote by $D(n_t)$ the system (3.2) truncated at n_t and, beginning with $D(2)$, several of the lower-order truncated systems will be investigated here to show the emergence of random trajectories as n_t is increased.

4.1. *The $D(2)$ system*

This system is given by

$$\dot{R}_1 = R_1 R_2 \sin(2\pi\Omega_1), \quad \dot{R}_2 = -R_1^2 \sin(2\pi\Omega_1),$$
$$2\pi\dot{\Omega}_1 = (2R_2 - R_1^2/R_2)\cos(2\pi\Omega_1). \tag{4.1}$$

The constants of motion are $J_1 + J_2 = 1$ and $h = R_1^2 R_2 \cos(2\pi\Omega_1)$. For the invariant set $\mathscr{S}_0$, the equations for R_1 and R_2 are equivalent to (2.4). On the other hand, $\mathscr{S}_m$ demands that

$$R_1/R_2 = 2^{\frac{1}{2}}. \tag{4.2}$$

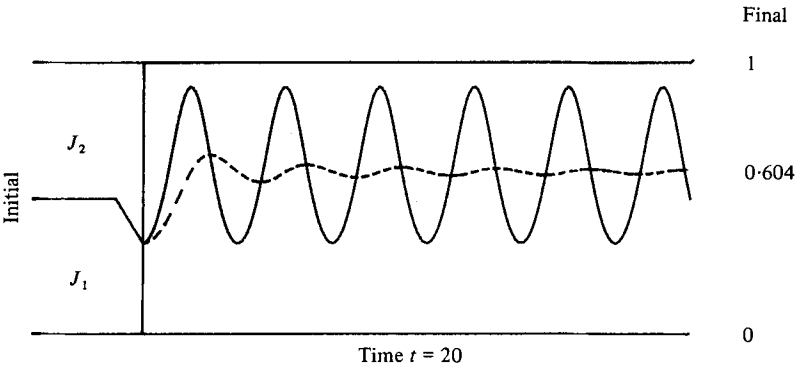

FIGURE 3. Evolution of $D(2)$ from the initial condition $R_1 = (\frac{1}{3})^{\frac{1}{2}}$, $R_2 = (\frac{2}{3})^{\frac{1}{2}}$, $\omega_1 = \frac{1}{8}$, and $\omega_2 = \frac{2}{8}$; ——, action; – – –, time-averaged action.

For the general solution, let us square both sides of the R_2 equation to obtain

$$(\dot{R}_2)^2 = R_2^4 - 2R_2^2 + 1 - h^2/R_2^2$$

with the use of the constants of motion. In action J_2, this gives rise to a differential equation

$$\tfrac{1}{4}(\dot{J}_2)^2 = J_2^3 - 2J_2^2 + J_2 - h^2,$$

satisfied by the Weierstrass elliptic functions. By a linear transformation $J_2 = \mathscr{P} + \frac{2}{3}$, we then obtain the normal form

$$(\dot{\mathscr{P}})^2 = 4(\mathscr{P} - e_1)(\mathscr{P} - e_2)(\mathscr{P} - e_3).$$

Here the three roots are

$$e_1 = \tfrac{2}{3}\cos(\tfrac{1}{3}\phi), \quad e_2 = \tfrac{2}{3}\cos(\tfrac{1}{3}\phi + 120°), \quad \text{and} \quad e_3 = \tfrac{2}{3}\cos(\tfrac{1}{3}\phi + 240°),$$

where $\phi = \cos^{-1}(27h^2/2 - 1)$. Suppose that the roots have been arranged as in $e_1 \geqslant e_2 \geqslant e_3$. Then the general solution for our problem is (Davis 1962, p. 157)

$$\mathscr{P} = e_3 + (e_2 - e_3)\,\mathrm{sn}^2[\lambda(t - t_0), \kappa], \tag{4.3}$$

where $\lambda^2 = e_1 - e_3$, $\kappa^2 = (e_2 - e_3)/(e_1 - e_3)$, and t_0 is the initial time constant.

To establish contact with the invariant sets, let us first examine the $h = 0$ case. Since $e_1 = e_2 = \frac{1}{3}$ and $e_3 = -\frac{2}{3}$, (4.3) degenerates to $\mathscr{P} = -\frac{2}{3} + \tanh^2(t - t_0)$ (because $\kappa = 1$) or $J_2 = \tanh^2(t - t_0)$, thereby recovering the previous result (2.5). In the opposite case of the maximum $h = 2/\sqrt{27}$, we find that $e_1 = \frac{2}{3}$ and $e_2 = e_3 = -\frac{1}{3}$; hence $\mathscr{P} = -\frac{1}{3}$ or $J_2 = \frac{1}{3}$ in agreement with (4.2). In general, J_2 (and/or J_1) is periodic because of the elliptic sine. As an example, consider the mid-value of $h^2 = \frac{2}{27}$, for which $e_1 = 3^{-\frac{1}{2}}$, $e_2 = 0$, and $e_3 = -3^{-\frac{1}{2}}$; hence

$$J_2 = \tfrac{1}{3}(2 - 3^{\frac{1}{2}}) + 3^{-\frac{1}{2}}\,\mathrm{sn}^2[\lambda(t - t_0), \kappa],$$

where $\lambda^2 = 2/3^{\frac{1}{2}}$ and $\kappa^2 = \frac{1}{2}$. Figure 3 gives the numerical result of evolving $D(2)$ from the initial condition, $R_1 = (\frac{1}{3})^{\frac{1}{2}}$, $R_2 = (\frac{2}{3})^{\frac{1}{2}}$, $\omega_1 = \frac{1}{8}$, and $\omega_2 = \frac{2}{8}$, which gives exactly $h^2 = \frac{2}{27}$. The periodic J_2 conforms to the analytic solution if t_0 is chosen as the quarter period of sn. In particular, the maximum and minimum of J_2 are found to be $\frac{2}{3}$ and $\frac{1}{3}(2 - 3^{\frac{1}{2}}) \simeq 0{\cdot}089$, respectively. Further, since the peaks (or troughs) of J_2 appear every $t \simeq 3{\cdot}45$ in the figure, one may estimate the half-period $\lambda \times 3{\cdot}45 \simeq 3{\cdot}71$, agreeing closely with the tabulated value of 3·7082 by Davis (1963, p. 176).

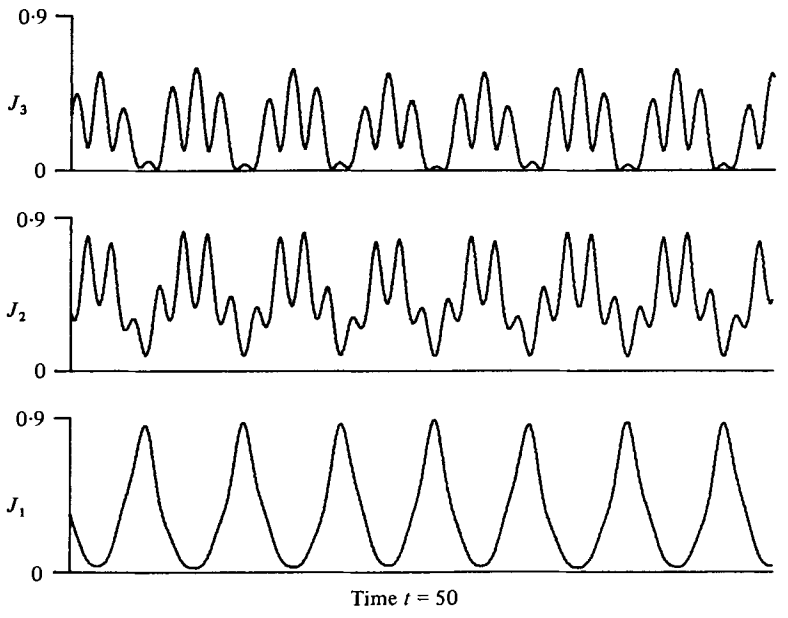

FIGURE 4. Actions of $D(3)$ evolved from the initial condition $I^{(3)}$.

Although patterned after (2.4), the system $D(2)$ does not at all exhibit unidirectional energy transfer. In fact, it is energy-sharing because the time-averaged actions

$$\bar{J}_n(t) = \frac{1}{t}\int_0^t J_n(s)\,ds, \tag{4.4}$$

are of comparable magnitude, as shown in figure 3. (Note that the long-time-averaged actions are the same for all trajectories with the same h, since they differ only by the constant t_0.)

4.2. *The $D(3)$ system*

The invariant set $\mathscr{S}_0$ of this system is precisely the unidirectional energy transfer model (2.8). Now solving the first two equations of (3.5) with R_4 suppressed, we obtain $R_1 = R_2 = 2R_3$ for the invariant set $\mathscr{S}_m$. Note that the equilibrium modal energy displayed in figure 2 of Kerr & Siggia (1978) is exactly that of $\mathscr{S}_m$. For a typical trajectory, we have evolved $D(3)$ from the initial condition $I^{(3)}$ which is defined by

$$I^{(m)} = \{R_n = m^{-\frac{1}{2}} \text{ and } \omega_n = \tfrac{1}{8}, \text{ for } n = 1, \ldots, m\}.$$

Since the time histories of J_n depicted in figure 4 are periodic, it is tentatively concluded that the present system has in general a periodic motion.

4.3. *The $D(4)$ system*

For the invariant set $\mathscr{S}_m$ of $D(4)$ we must solve (3.5) with R_5 suppressed. In terms of R_2, we find that $R_1 = R_2(3 \mp 5^{\frac{1}{2}})^{\frac{1}{2}}$, $R_3 = \frac{1}{2}R_2(-1 \pm 5^{\frac{1}{2}})$, and $R_4 = \frac{1}{8}R_2(-1 \pm 5^{\frac{1}{2}})^2$. The upper signs correspond to the equilibrium modal energy given in figure 2 of Kerr & Siggia (1978).

To exhibit typical trajectory behaviour, $D(4)$ has been evolved from the initial condition $I^{(4)}$; the result is presented in figure 5. First of all, the phase plots of Re (u_n)

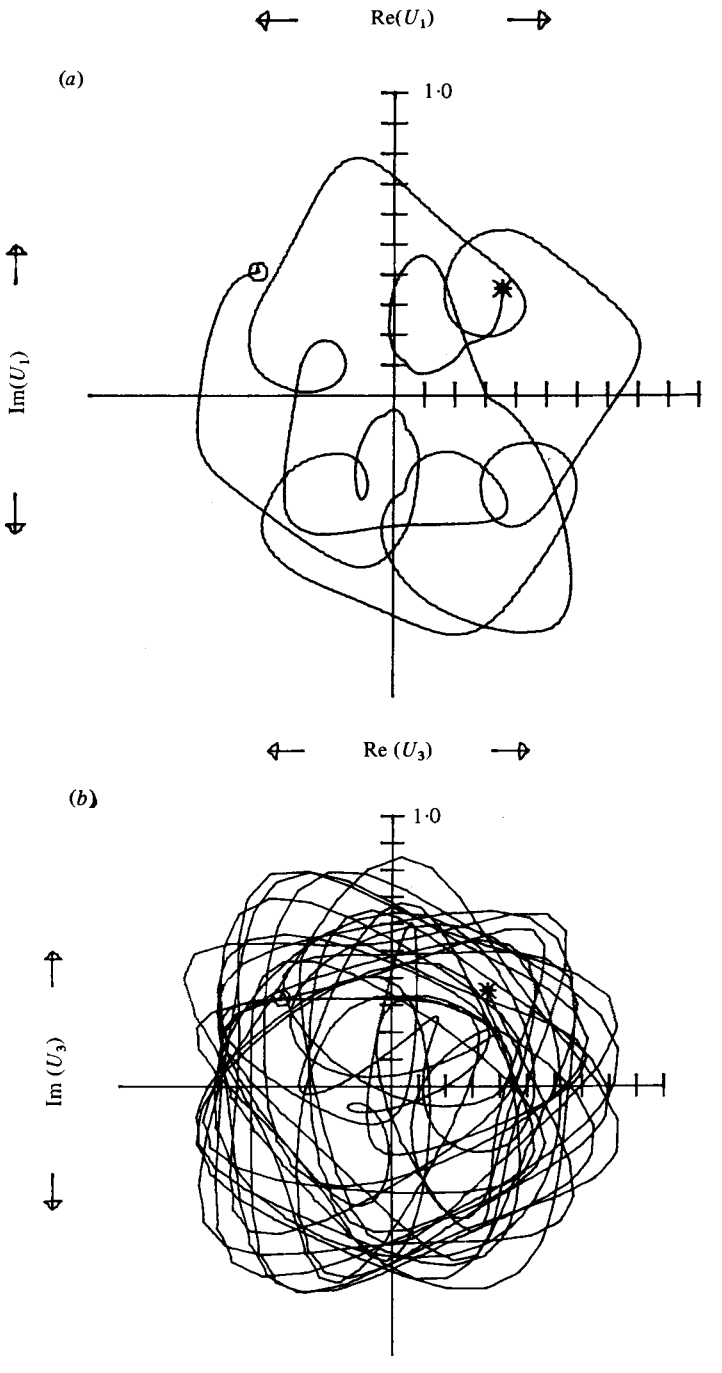

FIGURE 5 (a, b). For legend see next page.

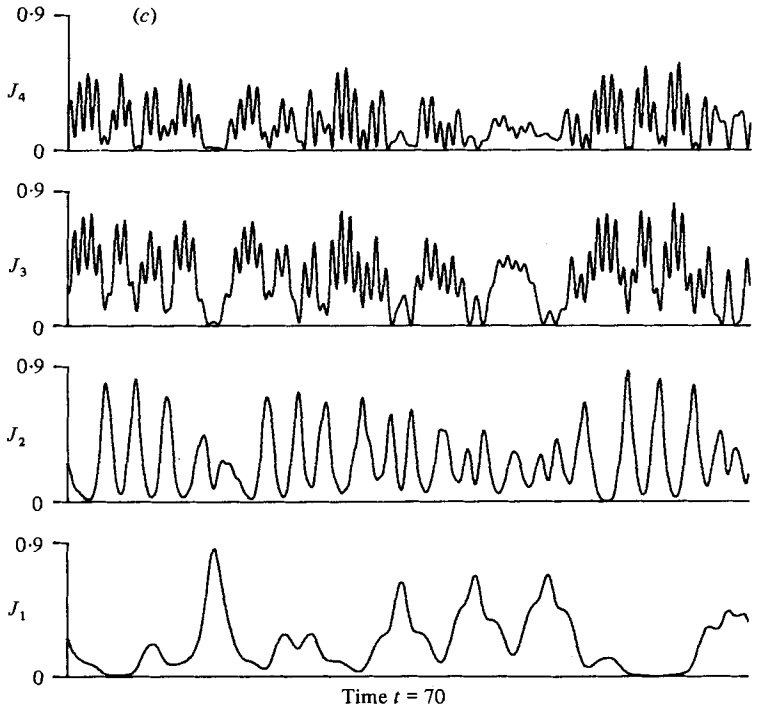

FIGURE 5. Evolution of $D(4)$ from the initial condition $I^{(4)}$ (evolution time = 70). (*a*) Phase plot of Re (u_1) *vs.* Im (u_1). (*b*) Phase plot of Re (u_3) *vs.* Im (u_3). (*c*) Actions.

vs. Im (u_n) shown in figures 5(*a*, *b*) develop quite an erratic pattern. Although both figures 5(*a*, *b*) contain trajectories of the same evolution time, the latter is more heavily traversed than the former because the characteristic time scale of u_3 is about an order of magnitude less than that of u_1 (see table 1). To suppress the effect of angle variables, we have presented in figure 5(*c*) the time histories of J_n, which clearly indicate that the motion is non-periodic in the evolution time of the figure.

It is indeed surprising to find that, going from $n_t = 3$ to 4, the trajectory has suddenly changed from a periodic to nonperiodic motion. This change may further be illustrated by the trajectory flow on a constant energy surface

$$\sum_{n=1}^{n_t} R_n^2 = 1.$$

On the energy sphere $R_1^2 + R_2^2 + R_3^2 = 1$, the trajectory of $D(3)$ can be parametrized by the polar and azimuthal angles (Lee 1979)

$$\theta_{123} = \tan^{-1}(R_1/R_2), \quad \xi_{123} = \tan^{-1}(R_2/R_3 \cos\theta_{123}). \tag{4.5}$$

When no isolating constant of motion exists besides energy, the trajectory flow will wander freely on the energy sphere; hence, the plot of θ_{123} *vs.* ξ_{123} would completely fill in the square with side $\frac{1}{2}\pi$ (in a numerical sense), since $R_n \geqslant 0$. Because of the cubic constant of motion h, this cannot however be so. In fact, as shown in figure 6, the trajectory flow of $D(3)$ is not only restricted to part of the energy sphere, but also stream-lined consistently with the apparent periodicity. Unfortunately, it is impossible

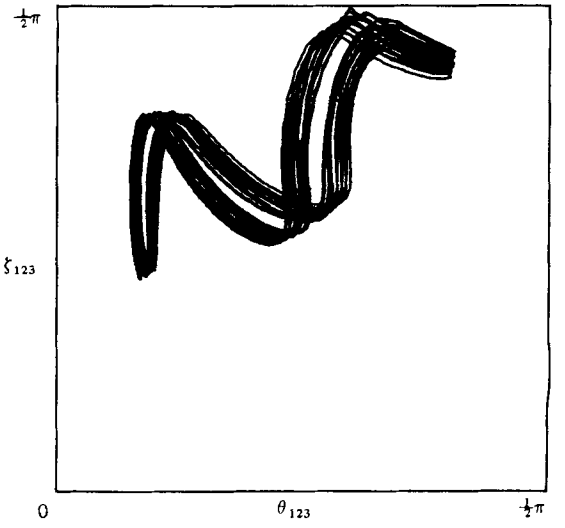

FIGURE 6. Trajectory flow on the constant-energy sphere of $D(3)$ evolved from the initial condition $I^{(3)}$ (evolution time = 100).

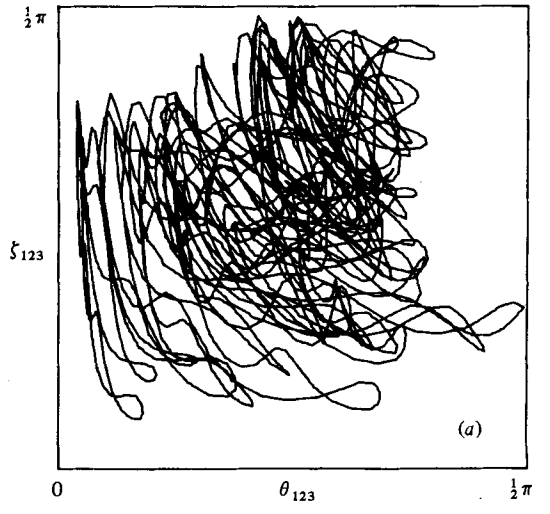

FIGURE 7 (*a*). For legend see next page.

to decide from figure 6 if the motion is periodic or quasi-periodic. Hence, the trajectory of $D(3)$ will be vaguely referred to as a periodic or quasi-periodic motion. As we now examine $D(4)$, the constant-energy surface is of dimension 4, yet one can sample three-dimensional projections of it by the polar and azimuthal angles defined similarly to (4.5). From the three-dimensional projections of figure 7, it is evident that the trajectory of $D(4)$ flows more freely on the energy surface than $D(3)$. Owing to the presence of h, however, one cannot infer from figure 7 if $D(4)$ is ergodic or not because the entire squares with side $\frac{1}{2}\pi$ are not accessible. Hence, the question of ergodicity will be approached by the decay property of the time-correlation functions of u_n, which will presently be carried out for $D(6)$.

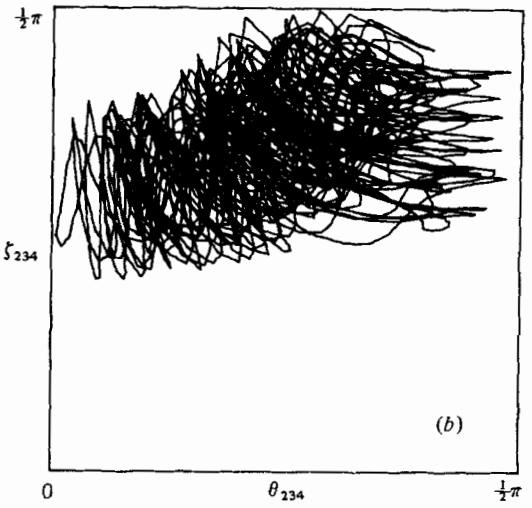

FIGURE 7. Trajectory flow on the constant-energy surface of $D(4)$ evolved from the initial condition $I^{(4)}$ (evolution time = 140). (*a*) Two-dimensional projection of θ_{123} *vs.* ξ_{123}. (*b*) Two-dimensional projection of θ_{234} *vs.* ξ_{234}.

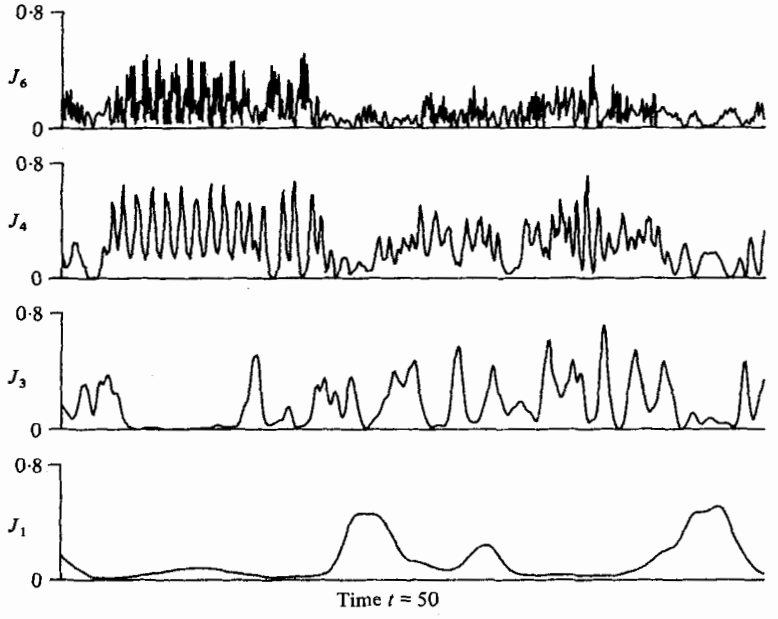

FIGURE 8. Actions of $D(6)$ evolved from the initial condition $I^{(6)}$.

4.4. *The $D(6)$ system*

Omitting the $D(5)$ system, we shall investigate here in detail the dynamical model $D(6)$, the trajectory of which is quite random and thereby typifies a higher-order truncated system $D(n_t)$ for $n_t > 6$. As shown in figure 8, the higher-order J_n fluctuate very rapidly and randomly in a time range in which J_1 has evolved a gradual but somewhat sporadic non-periodic motion. In any event, it is more meaningful to examine the

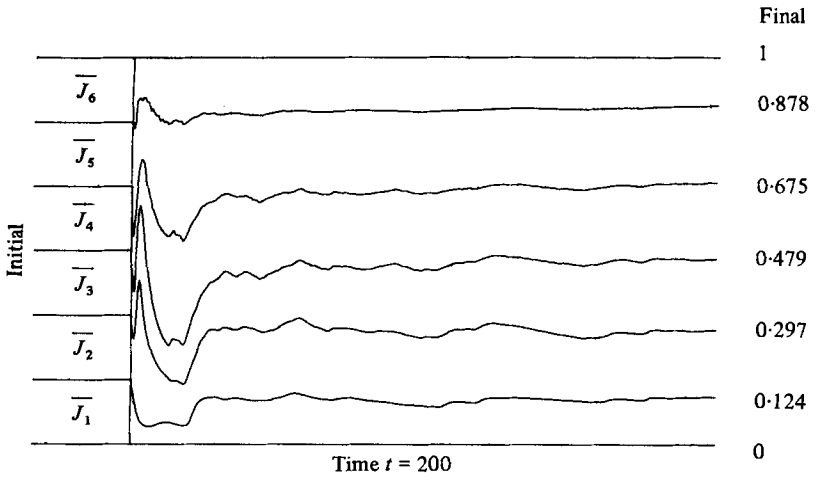

FIGURE 9. Time-averaged actions of $D(6)$ evolved from the initial condition $I^{(6)}$.

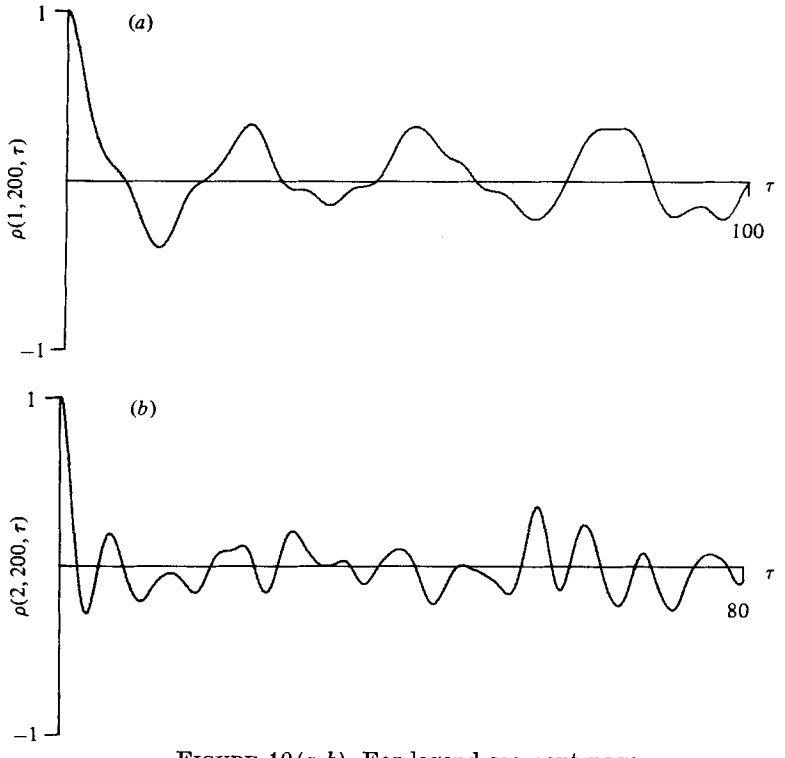

FIGURE 10(a,b). For legend see next page.

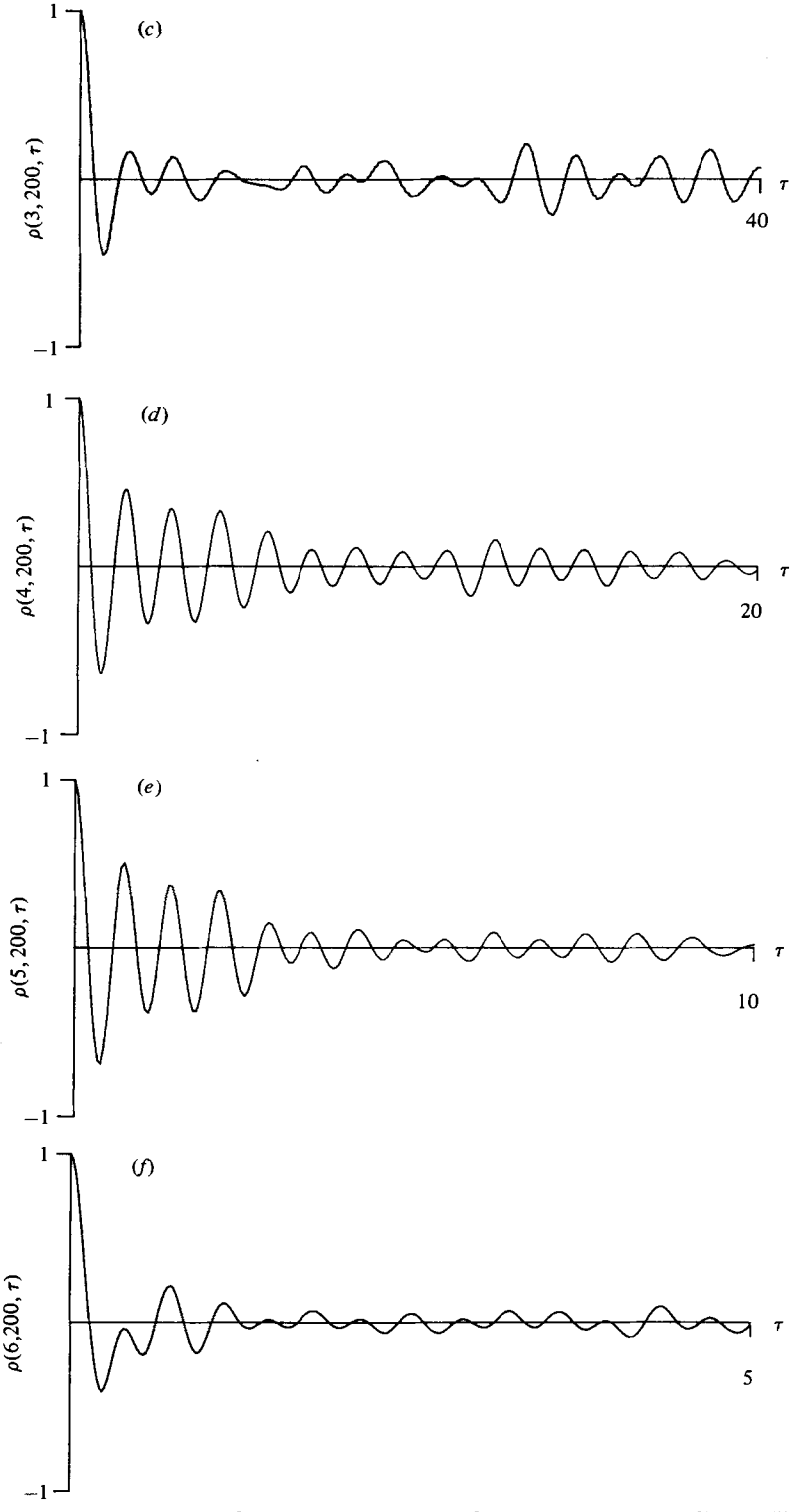

FIGURE 10. Autocorrelations of Re (u_n) of $D(6)$ evolved from the initial condition $I^{(6)}$ for the total evolution time $T = 200$. (*a*) $\rho(1, 200, \tau)$; (*b*) $\rho(2, 200, \tau)$; (*c*) $\rho(3, 200, \tau)$; (*d*) $\rho(4, 200, \tau)$; (*e*) $\rho(5, 200, \tau)$; (*f*) $\rho(6, 200, \tau)$.

n	1	2	3	4	5	6
Characteristic time	26·67	6·93	2·85	1·36	0·70	0·36

TABLE 1. Characteristic correlation times of the system $D(6)$.

time-averaged actions computed by (4.4). Figure 9 shows that $\bar{J}_n$ settle down to steady-state values after a long evolution time ($t = 200$). Furthermore, they exhibit a good measure of energy-sharing among all six modes.

The degree of randomness may be quantified by an autocorrelation of the type defined by Kells & Orszag (1978)

$$\rho(n, T, \tau) = \int_0^{T-\tau} \mathrm{Re}\,[u_n(s)]\,\mathrm{Re}\,[u_n(s+\tau)]\,ds \Big/ \int_0^{T-\tau} \{\mathrm{Re}\,[u_n(s)]\}^2\,ds,$$

which satisfies $\rho(n, T, 0) = 1$. (Although the time correlations for $\mathrm{Im}\,(u_n)$ can be defined similarly, they exhibit more or less the same decay behaviour as $\rho(n, T, \tau)$, and hence will not be considered here explicitly.) Taking the evolution time $T = 200$ as sufficiently long, we have computed autocorrelations from the trajectory of figure 9. All correlations (figure 10) first fall off rapidly but then undergo oscillations without damping out completely. Hence, in general the motion of $D(6)$ is quite random, but not sufficiently so to be mixing in phase space (Lebowitz 1972). In particular, the oscillation amplitudes are quite small for $\rho(5, T, \tau)$ and $\rho(6, T, \tau)$. Hence, the motion of higher-order u_n is almost mixing, although the motion of lower-order modes is far from it. A quantitative estimate of characteristic times can be obtained from the oscillations, as shown in table 1. In comparison to characteristic correlation times, it is inferred that $T = 200$ is indeed a long evolution time for all but $\rho(1, T, \tau)$. It is a well-known fact (Monin & Yaglom 1975, p. 340) that in fully developed turbulence the characteristic time scale of a typical eddy decreases with decreasing eddy size. The present cascade model indeed supports this: the characteristic time decreases roughly by half as n ($\geqslant 2$) is increased by one. In other words, by halving (doubling) the eddy size (wavenumber) the characteristic correlation time is halved. Hence, the dynamical model $D(n_t)$ is numerically a stiff differential system with widely varying time scales (Lapidus, Aiken & Liu 1974).

Summing up, going from $n_t = 3$ to 4 the trajectory of $D(n_t)$ changes abruptly from periodic or quasi-periodic to non-periodic. The non-periodic motion of $D(4)$ is only modestly chaotic. As n_t is further increased to 6 and larger (the results of $D(9)$ will not be presented here), the random motion of higher-order u_n almost becomes mixing, although the non-periodic motion of lower-order u_n does not. The motion of $D(n_t)$, therefore, has a layered structure in that big eddies (lower-order u_n) evolving slowly but sporadically coexist with a sequence of small eddies (higher-order u_n) which undergo more rapid and chaotic fluctuations with the decreasing eddy size. In the present inviscid case, all modes participate energetically, as exhibited by energy-sharing of the time-averaged actions. (This should, however, be distinguished from energy-equipartitioning, which calls for the mixing property.)

Although we have thus far restricted ourselves to one type of initial conditions $I^{(n_t)}$, the dynamical conclusions remain valid for other arbitrary initial conditions.

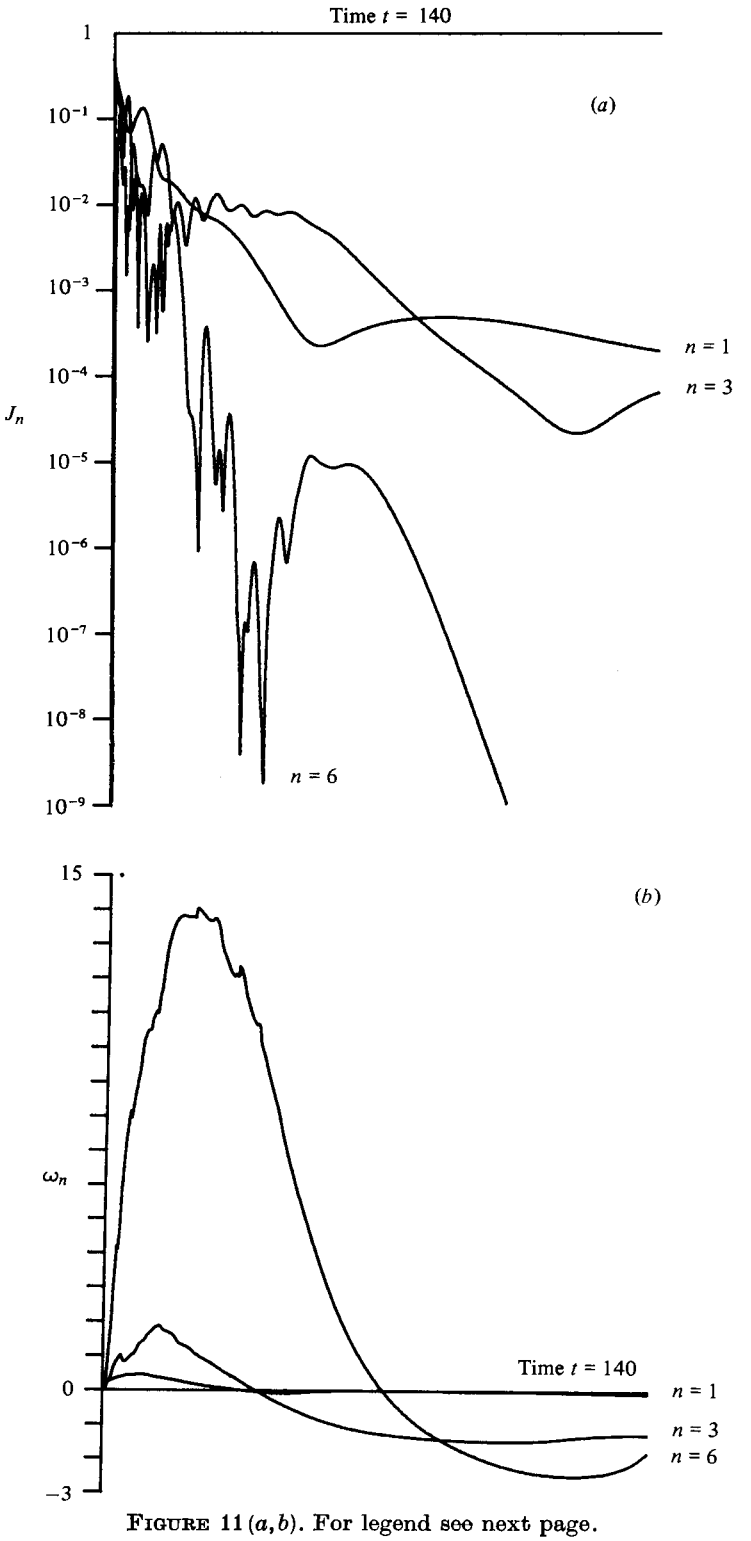

FIGURE 11 (a, b). For legend see next page.

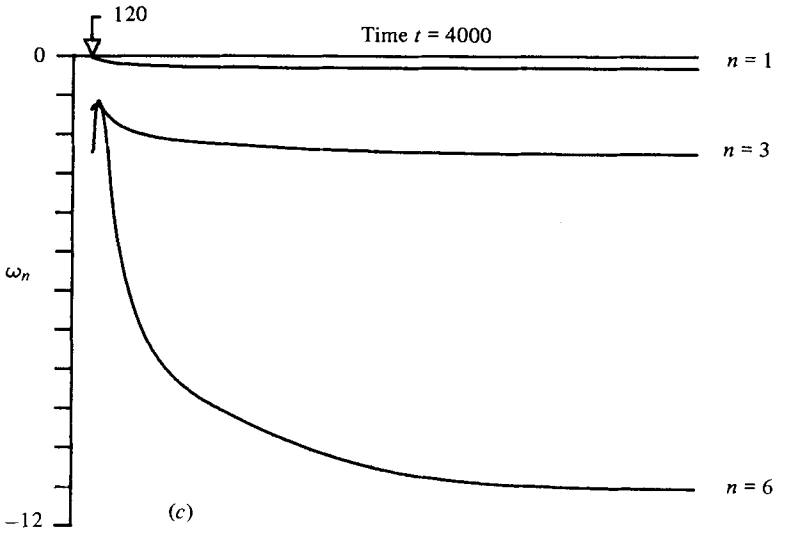

FIGURE 11. Free-decay dynamics of (3.1) evolved from the initial condition I_3 under $n_t = 6$ and $\nu = 1 \times 10^{-3}$. (*a*) Actions for $n = 1$, 3 and 6; (*b*) angles for $n = 1$, 3 and 6; (*c*) long-time evolution of the angles.

There is, however, one exception: a class of initial conditions defined by

$$I_2 = \{R_1 = 1, \omega_1 = \text{arbitrary, and } R_n = \omega_n = 0\,(2 \leqslant n \leqslant n_t)\}$$

gets mapped into the invariant set $\mathscr{S}_0$ (appendix).

5. The steady equilibrium state of model (3.1)

Having established inviscid equilibrium solutions, we are now in a position to examine the steady-state dynamics of model (3.1) sustained by introducing energy into the first mode at the same rate as viscous dissipation. Although (3.1) is an unclosed system, there is an effective upper truncation limit based on a Kolmogorov's length scale, beyond which the contribution of all truncated modes can safely be ignored (§ 2.2). In this section, we shall be concerned with another initial condition $I_3 = \{R_1 = R_2 = 2^{-\frac{1}{2}}, \omega_1 = \omega_2 = \frac{1}{8}, \text{ and } R_n = \omega_n = 0 \text{ for } n = 3, \ldots, n_t\}$, which is an extension of I_1 to the complex case.

5.1. *Free decay*

As a logical intermediate step, we shall investigate the free decay dynamics in the absence of an energy input ($\epsilon_f = 0$). We have evolved system (3.1) truncated at $n_t = 6$ from the initial condition I_3 under $\nu = 1 \times 10^{-3}$. But figure 11 presents only J_n and ω_n for $n = 1$, 3, and 6, for the others behave similarly. First, J_3 and J_6 build up rapidly from the initial zero due to the nonlinear interaction, but all J_n have decayed substantially at the final time of figure 11 (*a*). A surprise here is the disappearance of fluctuations beyond $t \simeq 50$; a major departure from the inviscid case (figure 8). The corresponding angles shown in figure 11 (*b*) also build up rapidly, but change their signs from plus to minus at $t \simeq 80$. It must be pointed out that the clockwise (counterclockwise) rotation is measured by the positive (negative) angle. Hence the rotating vectors $R_n \exp(i2\pi\omega_n)$ apparently change the sense of rotation, the significance of

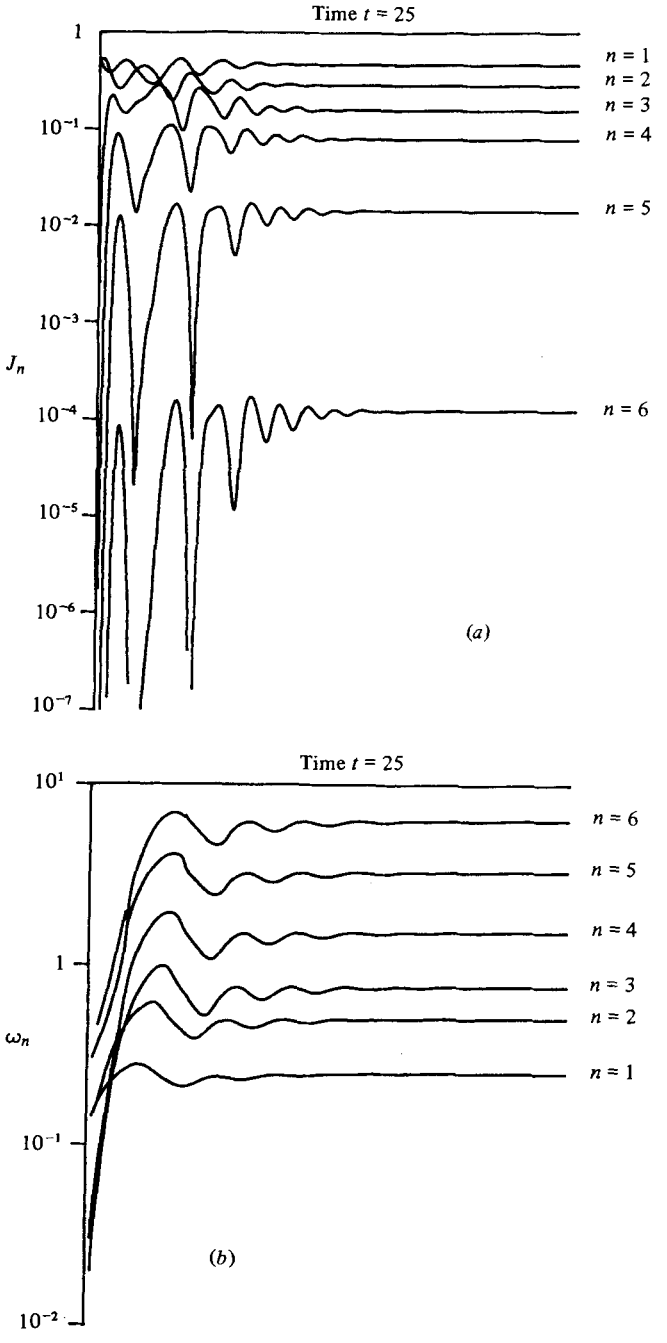

FIGURE 12. Stationary dynamics of (3.1) evolved from the initial condition I_3 under $n_t = 6$ and $\nu = 0{\cdot}02$. (*a*) Actions. (*b*) Angles.

which is not clear at present. To determine the asymptotic result, we have continued the evolution of ω_n far beyond the time range of figure 11 (*b*). It is very surprising to find from figure 11 (*c*) that the ω_n settle down to constant values, implying that the rotating vectors eventually cease to rotate. Therefore, the overall picture of free decay is this: Initially the rotating vectors for $n \geqslant 3$ spiral out very rapidly owing to the energy fed in by u_1 and u_2, and then all rotating vectors begin to spiral in towards the origin of the phase plots of $\mathrm{Re}\,(u_n)$ *vs.* $\mathrm{Im}\,(u_n)$, thereby reflecting dissipation. At $t \simeq 80$ the sense of rotation changes from clockwise to counter-clockwise directions. After a long time ($t > 2000$), however, the rotating vectors cease to rotate; hence they will all shrink into the origin but without rotating around the origin of the phase space.

It must be pointed out that ν and n_t used here have been chosen arbitrarily without regard to $\alpha_k = (\epsilon_\nu/\nu^3)^{\frac{1}{4}}$. Although at the very initial instance ($t \simeq 3$) the dissipation $\alpha_k (\simeq 130)$ can exceed the truncation $\alpha_t (= 32)$, it is found that $\alpha_k \ll \alpha_t$ for all $t > 20$, for α_k decreases continually due to the energy dissipation. Inasmuch as the long-time behaviour is concerned, therefore, the present truncation is consistent.

5.2. *Equilibrium cascade flow of modal energies*

In free decay, the choice of ν and n_t was not critical because α_k will eventually fall below α_t. On the other hand, in a stationary flow the α_k will approach a constant value; hence the consistency of truncation must be assured by $\alpha_k < \alpha_t$ for all t. Although ν and n_t can be varied separately, we shall examine here the consequences of consistent and inconsistent truncations by varying ν for a fixed n_t.

Consistent truncation ($\alpha_k < \alpha_t$). The model (3.1) truncated at $n_t = 6$ was evolved from the initial condition I_3 under $\nu = 0{\cdot}02$. Since ϵ_f is not known *a priori*, the J_1 was boosted at the end of each integration time step to maintain

$$\sum_{n=1}^{6} J_n = 1$$

(§ 2.2). The numerical results are very surprising. First of all, figure 12 (*a*) shows that after a rapid build-up of J_n for $n \geqslant 3$ from the initial zero, all J_n undergo a rather violent oscillation, reminiscent of the inviscid solution (figure 8). Afterwards, they begin to settle down at $t \simeq 10$ and a steady equilibrium energy state is attained at the final time of the figure. Second, the key information is provided by figure 12 (*b*) in which the steady-state values of ω_n give rise to $\Omega_n = \pm\frac{1}{4}, \pm\frac{3}{4}$ for $n = 1, \ldots, 5$. This therefore implies that when the energy input and dissipation are in balance the cascade system (3.1) evolves towards a stationary equilibrium state which is precisely the invariant set $\mathscr{S}_0$ defined by (3.4). And this equilibrium state has been found attainable from an arbitrary initial condition with $R_1 \neq 0$ and $R_2 \neq 0$.

After equilibration the energy input and dissipation rates coincide, i.e.

$$\epsilon_f = \epsilon_\nu \simeq 0{\cdot}514.$$

One then finds $\alpha_k \simeq 15{\cdot}9$, which is about half the truncation α_t; hence the consistency of truncation is checked *a posteriori*.

Ambivalent truncation ($\alpha_k \simeq \alpha_t$). As we repeat the computation of figure 12 but under a smaller $\nu = 0{\cdot}005$, it turns out that $\alpha_k \simeq 43$ which is somewhat larger than $\alpha_t = 32$. One therefore expects that the effect of inviscid solutions would be felt mildly on the otherwise steady equilibrium state of $\mathscr{S}_0$. In fact, figure 13 shows the

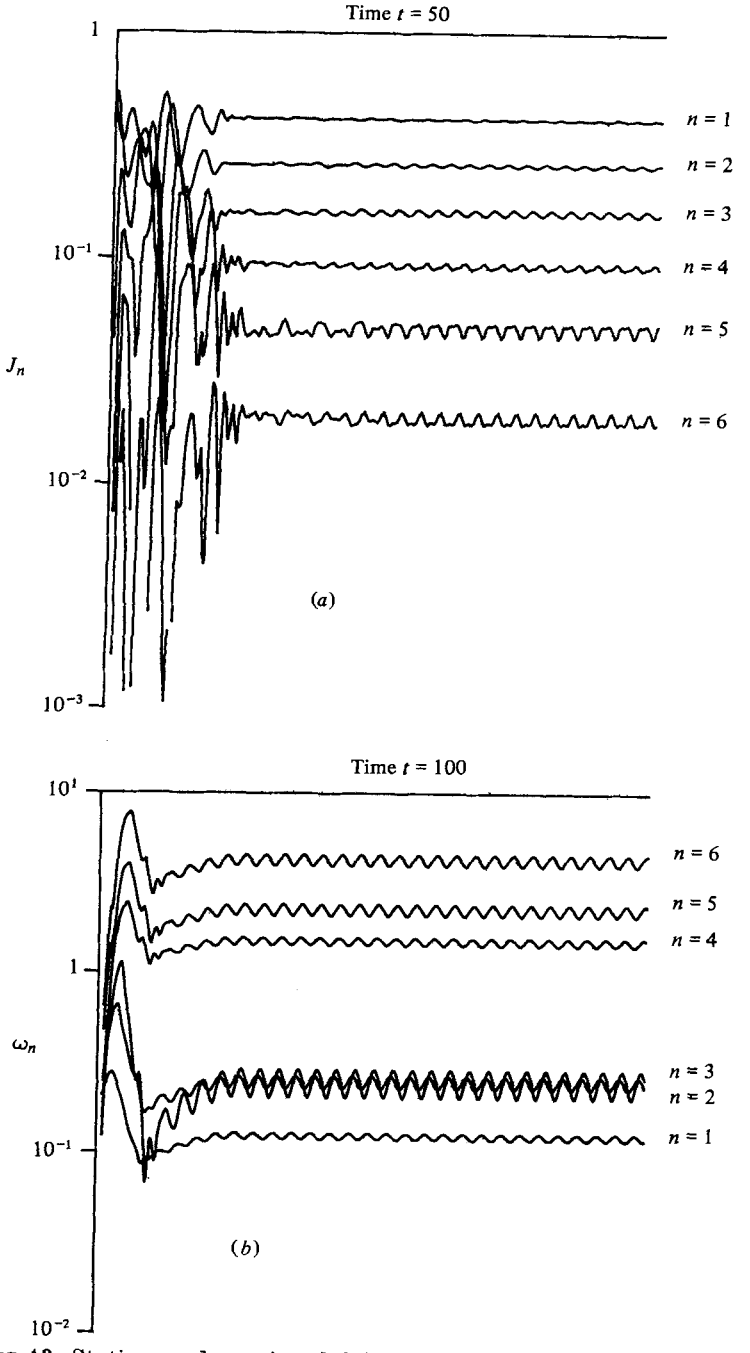

FIGURE 13. Stationary dynamics of (3.1) evolved from the initial condition I_3 under $n_t = 6$ and $\nu = 0{\cdot}005$. (*a*) Actions. (*b*) Angles.

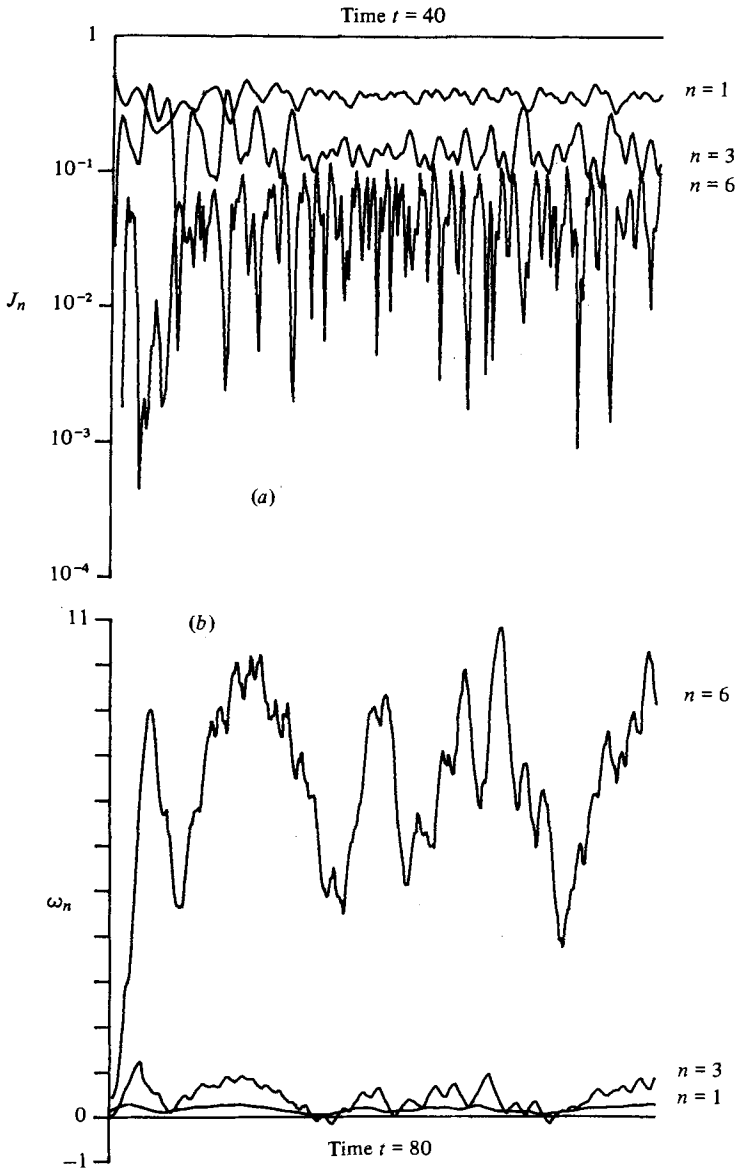

FIGURE 14. Stationary dynamics of (3.1) evolved from the initial condition I_3 under $n_t = 6$ and $\nu = 0{\cdot}002$. (*a*) Actions for $n = 1$, 3 and 6. (*b*) Angles for $n = 1$, 3 and 6.

same overall behaviour of J_n and ω_n of figure 12; the main difference being persisting oscillations even after the initial equilibration period.

Inconsistent truncation ($\alpha_k > \alpha_t$). As ν is further decreased, the dissipation range lies mostly beyond α_t, so that to a good measure the present problem resembles the inviscid flow of § 4. This has clearly been substantiated by figure 14, which depicts the time histories of J_n and ω_n for $n = 1$, 3, and 6, evolved under $\nu = 0{\cdot}002$. Note that both actions (figure 14*a*) and angles (figure 14*b*) undergo a violent fluctuation; in particular, the fluctuating J_3 and J_6 may be compared with the inviscid counterparts in figure 8. Consequently, the energy dissipation rate fluctuates, and so does α_k in

the range of 57–92, which is well above $\alpha_t = 32$. Under the present inconsistent truncation, therefore, the equilibrium dynamics exhibit more of the chaotic motion of inviscid solutions than the stable motion of $\mathscr{S}_0$.

To show that ν and n_t play an interchangeable role, we have repeated the computation of figure 14 but with a larger $n_t = 9$. Although not shown here explicitly, it has been found that the cascade model (3.1) again evolves arbitrary initial conditions into the invariant set $\mathscr{S}_0$ just as in figure 12. This is because $\alpha_k \simeq 84$ turns out much less than $\alpha_t = 256$, hence the spurious effect of inviscid solutions has been suppressed altogether.

6. Concluding remarks

We have investigated the two cascade models formally derived from Burgers' equation. The first model (2.9) produces no fluctuations, for its trajectory is identical to that of the Desnyansky–Novikov model. The second cascade model (3.1) has also proved unable to produce fluctuations because when truncated consistently it maps an arbitrary initial point into the invariant set which is the attainable phase space of the first model. On the other hand, when truncated inconsistently the trajectory of (3.1) develops an erratic and sporadic motion, thereby reflecting the apparently chaotic motion of inviscid energy-sharing solutions. Although (3.1) has the same nonlinear terms as the Kerr–Siggia model, there is a very significant difference between them (Siggia 1979, private communication). Unlike the natural viscous terms in (3.1), the Kerr–Siggia model relegates all energy dissipation to the upper truncation mode by an artificial eddy damping. Hence, under a stationary energy excitation, the Kerr–Siggia model displays the symptom of inconsistent truncation because the natural flow of energy has been blocked off towards the Kolmogorov dissipation range. For this reason, the emergence of temporally intermittent fluctuations by Kerr–Siggia model is not a faithful reflexion of cascade dynamics. Rather, it is due to the particular mode of energy damping imposed by that model.

Notwithstanding, the second cascade model has a very peculiar long-time behaviour. The inviscid (conservative) model develops a random motion with strong tendency towards energy-sharing. Now, as we introduce viscosity, however small it may be, the trajectory loses its randomness; hence, the motion becomes laminar (stable) after a long evolution time. This sort of long-time behaviour contradicts an intuitive feeling that viscosity should not completely obliterate the random behaviour of a turbulence model. Whether it is just a quirk of the present cascade model or something common to the Navier–Stokes equations must be investigated. From the standpoint of modelling, however, emergence of a stable asymptotic trajectory is not unprecedented. For instance, two Burgers models for a stationary channel flow have been found to evolve respectively into an equilibrium point in phase space (Lee 1971) and a limit cycle (Lee 1972), beyond the laminar–turbulent transition. This should, of course, be contrasted with Lorenz's (1963) thermal convection model developing a non-periodic motion around the laminar equilibrium points.

I wish to thank Eric Siggia for pointing out to me the difference in his and our cascade model's viscous terms and independently verifying the difference in asymptotic dynamical behaviour. I also greatly benefited from the referee's reports.

Appendix. Entrapment of trajectory in the invariant set $\mathscr{S}_0$

To show that $D(n_t)$ maps the initial condition I_2 into the invariant set $\mathscr{S}_0$, it suffices to consider the lowest-order case of $D(2)$ written in rectangular form:

$$\begin{aligned} \dot{u}_1^r &= u_1^r u_2^i - u_1^i u_2^r, \quad & \dot{u}_1^i &= -u_1^r u_2^r - u_1^i u_2^i, \\ \dot{u}_2^r &= 2u_1^r u_1^i, & \dot{u}_2^i &= -(u_1^r)^2 + (u_1^i)^2, \end{aligned} \tag{A 1}$$

where $u_n = u_n^r + iu_n^i$. The appropriate initial condition is

$\{u_1^r = a_r/A^{\frac{1}{2}}$, $u_1 = a_i/A^{\frac{1}{2}}$, where $A = a_r^2 + a_i^2$ for the arbitrary a_r and a_i, $u_2^r = u_2^i = 0\}$.

Integration of (A 1) over a time step Δt yields

$$u_1^r = a_r/A^{\frac{1}{2}}, \quad u_1^i = a_i/A^{\frac{1}{2}}, \quad u_2^r = 2\Delta t a_r a_i/A, \quad u_2^i = \Delta t(a_i^2 - a_r^2)/A. \tag{A 2}$$

For the evolved state (A 2), we therefore have

$$\tan(2\pi\omega_1) = a_i/a_r \quad \text{and} \quad \tan(2\pi\omega_2) = (a_i^2 - a_r^2)/2a_r a_i.$$

Now, beginning from $\tan(4\pi\omega_1)$, we obtain the following equalities,

$$\tan(4\pi\omega_1) = \frac{2\tan(2\pi\omega_1)}{1-\tan^2(2\pi\omega_1)} = \frac{2a_r a_i}{a_r^2 - a_i^2} = \frac{-1}{\tan(2\pi\omega_2)} = \tan(2\pi\omega_2 \pm \tfrac{1}{2}\pi), \tag{A 3}$$

the first and last of which are due to the trigonometric identities. We then find from (A 3) that $\Omega_1 \equiv 2\omega_1 - \omega_2 = \pm\frac{1}{4}$; hence the evolved state (A 2) is indeed in $\mathscr{S}_0$, and so are the further evolved states by the definition of the invariant set. By a similar procedure including higher-order terms in Δt, one can show that the trajectory of $D(n_t)$ is confined to the invariant set $\mathscr{S}_0$.

REFERENCES

Bell, T. L. & Nelkin, M. 1977 *Phys. Fluids* **20**, 345.

Bell, T. L. & Nelkin, M. 1978 *J. Fluid Mech.* **88**, 369.

Byrd, P. F. & Friedman, M. D. 1954 *Handbook of Elliptic Integrals for Engineers and Physicists.* Springer.

Davis, H. T. 1962 *Introduction to Nonlinear Differential and Integral Equations*, cha. 6 and 7. Dover.

Desnyansky, V. N. & Novikov, E. A. 1974*a* *Prikl. Mat. Mekh.* (transl. *J. Appl. Math. Mech.*) **38**, 507.

Desnyansky, V. N. & Novikov, E. A. 1974*b* *Izv. Akad. Nauk S.S.S.R., Fiz. Atmos. Okean.* (transl. *Atmos. Ocean. Phys.*) **10**, 127.

Kamke, E. 1943 *Differentialgleichungen, Lösungsmethoden und Lösungen.* Akademische.

Kells, L. C. & Orszag, S. A. 1978 *Phys. Fluids* **21**, 162.

Kerr, R. M. & Siggia, E. D. 1978 *J. Stat. Phys.* **19**, 543.

Lamb, H. 1943 *Higher Mechanics.* Cambridge University Press.

Lapidus, L., Aiken, R. C. & Liu, Y. A. 1974 In *Stiff Differential Systems* (ed. R. A. Willoughby), p. 187. Plenum.

Lebowitz, J. L. 1972 In *Statistical Mechanics: New Concepts, New Problems, New Applications* (ed. S. A. Rice, K. F. Freed & J. C. Light), p. 41. University of Chicago Press.

Lee, J. 1971 *J. Fluid Mech.* **47**, 321.

Lee, J. 1972 *Phys. Fluids* **15**, 540.

LEE, J. 1979 *Phys. Fluids* **22**, 40.

LORENZ, E. N. 1960 *Tellus* **12**, 243.

LORENZ, E. N. 1963 *J. Atmos. Sci.* **20**, 130.

MONIN, A. S. & YAGLOM, A. M. 1975 *Statistical Fluid Mechanics*, vol. 2. Massachusetts Institute of Technology Press.

ORSZAG, S. A. 1977 In *Fluid Dynamics* (ed. R. Balian & J.-L. Peube). Gordon and Breach.

SIGGIA, E. D. 1977 *Phys. Rev.* A **15**, 1730.

SIGGIA, E. D. 1978 *Phys. Rev.* A **17**, 1166.